TISSUE ENGINEERING: Part A
Volume 25, Numbers 13 and 14, 2019

DOI: 10.1089/ten.tea.2018.0140

termis
Tissue Engineering
& Regenerative Medicine
International Society

ORIGINAL ARTICLE

Effect of Biomaterial Electrical Charge on Bone Morphogenetic Protein-2-Induced *In Vivo* Bone Formation

Maurits G.L. Olthof, MD,[1–4] Diederik H.R. Kempen, MD, PhD,[5] Xifeng Liu, PhD,[1,2] Mahrokh Dadsetan, PhD,[1,2] Marianna A. Tryfonidou, DVM, PhD,[3] Michael J. Yaszemski, MD, PhD,[1,2] Wouter J.A. Dhert, MD, PhD,[3,4] and Lichun Lu, PhD[1,2]

Biomaterials that act as both protein delivery vehicle and scaffold can improve the safety and efficacy of bone morphogenetic protein-2 (BMP-2) for clinical applications. However, the optimal scaffold characteristics are not known. The osteoinductive and osteoconductive capacity of a fixed electrically charged surface is thus far unexplored. Therefore, in this study, we aim to investigate the effect of different electrical states on BMP-2-induced bone formation in oligo[(polyethylene glycol) fumarate] (OPF) hydrogels. Neutral, negatively, or positively charged scaffolds were fabricated using unmodified OPF (neutral charge), sodium methacrylate crosslinked OPF (negative charge), or [2-(methacryloyloxy) ethyl] trimethylammonium chloride crosslinked OPF (positive charge), respectively. To allow investigation of surface charge for different BMP-2 release rates, three BMP-2 release profiles were generated by protein encapsulation into poly(lactic-co-glycolic acid) microspheres and/or adsorption on the OPF composite. Release of radiolabeled ^{125}I-BMP-2 was analyzed *in vitro* and *in vivo* and bone formation was assessed after 9 weeks of subcutaneous implantation in rats. Negatively charged OPF generated significantly more bone formation compared with neutral and positively charged OPF. This effect was seen for all three loading methods and subsequent BMP-2 release profiles. Along with charge modifications, a more sustained release of BMP-2 improved overall bone formation in OPF composites. Overall, this study clearly shows that negative charge enhances bone formation compared with neutral and positive charge in OPF composites.

Keywords: electrical charge, bone morphogenetic protein-2 release, biomaterials, bone tissue engineering, oligo[(polyethylene glycol) fumarate], poly(lactic-co-glycolic acid)

Impact Statement

Biomaterials can play a dual role in bone regeneration: they enable local sustained delivery of growth factors, such as bone morphogenetic protein-2 (BMP-2), while they provide structural support as scaffold. By better imitating the properties of native bone tissue, scaffolds may be both osteoconductive and osteoinductive. The latter can be achieved by modifying the electrical charge of the surface. The present work uses tunable oligo[(polyethylene glycol) fumarate] hydrogel and demonstrates that negative charge enhances BMP-2-induced bone formation compared with neutral or positive charge. Altogether, this indicates that tissue-specific surface charge modifications of biomaterials hold great promise in the field of tissue regeneration.

Introduction

Bone morphogenetic protein-2 (BMP-2) is a potent osteoinductive growth factor, which has shown impressive results in many preclinical bone regeneration studies.[1] Despite these encouraging results, clinical use of BMP-2 is complicated by its short biological half-life, lack of long-term stability, and tissue selectivity.[2] Therefore, local delivery of BMP-2 is essential for the effectiveness of growth factor. Several studies showed that local BMP-2 retention in carriers improved its osteoinductive capacity compared with injection of the carrier-free growth factor

Departments of [1]Physiology and Biomedical Engineering and [2]Orthopedic Surgery, Mayo Clinic College of Medicine, Rochester, Minnesota.
[3]Faculty of Veterinary Medicine, Utrecht University, Utrecht, The Netherlands.
[4]Department of Orthopaedics, University Medical Center, Utrecht, The Netherlands.
[5]Department of Orthopaedic Surgery, OLVG, Amsterdam, The Netherlands.

solution.[3–5] Consequently, many BMP-2 vehicles are under development to enhance the osteoinductive potential.

The newly developed biomaterials should not only function as a local BMP-2 delivery vehicle but also as a scaffold to support cell attachment, proliferation, and differentiation. These scaffold properties can act synergistically with the growth factor during bone regeneration and optimizing scaffold properties can improve the safety and efficacy of BMP-2 in future clinical applications. However, there is no consensus on the optimal scaffold characteristics for bone tissue engineering purposes. Development of an optimal interface between bone and biomaterials has taken place for many years.[6,7] Many studies have investigated the optimal bone/implant interface by alteration of biomaterial surface properties such as surface physical properties,[8,9] surface chemistry,[10] surface charge,[11,12] and surface functionalism.[13–15] Recently, surface charge generation by electrical polarization has drawn much attention.

Piezoelectricity is charge that is generated due to applied stress to a material or vice versa.[16] Previous research showed that the piezoelectric characteristics of bone directly influence bone formation.[11,17–19] Whereas bone can grow more efficiently under compression, tension can cause resorption. Even more so, when an electrical current was supplied, higher amounts of bone were observed at the negatively charged pole.[20] When these piezoelectric characteristics were applied to biomaterials (barium titanate [$BaTiO_3$], hydroxyapatite [HAp]/$BaTiO_3$, and poly(L-lactide) [PLLA]), *in vivo* results showed improved osteointegration in all biomaterials.[21–23] A more permanent electrically polarized material, such as Teflon, showed accelerated osteointegration and bone first formed at the negative pole, growing toward the positive pole.[12,24]

Furthermore, electrically polarized bioactive HAp showed improved osteointegration at the negatively charged surface pole.[25–27] Since electrical polarization showed improved bone formation at negatively charged surfaces of different biomaterials, functionalizing polymer surface with fixed negative electrical charge could in theory enhance any biomaterial's osteoconductive and osteoinductive properties.

Previously, oligo[(polyethylene glycol) fumarate] (OPF) networks were modified with charged small monomers containing negative (sodium methacrylate [SMA]) and positive (2-(methacryloyloxy) ethyl)-trimethyl ammonium chloride [MAE]) charges to create hydrogels with different charges.[28] The monomers were successfully incorporated in the polymer networks and Zeta potential measurements showed that the polymer networks were electrically charged and conductive, which increased with higher concentrations of monomers.[28] The modified hydrogels became sensitive to the pH and ionic strength of their environment.

Furthermore, cells cultured on the modified hydrogels not only remained viable but cellular behavior was also influenced by the modification. Whereas positively charged OPF promoted *in vitro* neurite outgrowth of primary nerve cells, negative charge stimulated *in vitro* attachment of chondrocytes.[28,29] Although the charge modifications influence *in vitro* cell behavior, it is not known whether charge also plays a role in three-dimensional (3D) *in vivo* tissue formation.

Considering the previous research on electrically charged materials, we hypothesized that a negative charged surface would better improve *in vivo* bone formation than positive or neutral charged surfaces. Therefore, the aim of this study is to investigate the effect of negative and positive charge on bone formation in OPF networks. Furthermore, the OPF hydrogels were used as BMP-2 delivery vehicles. Since the hydrogel charge could also affect BMP-2 release and hence influence bone formation, BMP-2 was incorporated in the differentially charged OPF scaffolds by protein adsorption and/or encapsulation into poly(lactic-co-glycolic acid) (PLGA) microspheres to vary the release kinetics. A previous study showed differential release of biologically active BMP-2 using this method in OPF.[30] This method allowed us to investigate the effect of surface charge on bone formation for different BMP-2 release rates.

Materials and Methods

Experimental design

OPF hydrogels (22.5% w/w) with a 75% (w/w) porosity containing 2.5% (w/w) PLGA microspheres were used for the BMP-2 containing implants as well as the BMP-2 unloaded controls. To analyze the effect of charge on BMP-2 release and bone formation, SMA (Sigma-Aldrich, St. Louis, MO) or MAE (Sigma-Aldrich, St. Louis, MO) were crosslinked into the OPF hydrogel to obtain either a fixed negative or positive charge, respectively (Fig. 1A, C). By adjusting the % of adsorbed BMP-2 on the composite matrix and BMP-2 encapsulated in PLGA microspheres, the release of BMP-2 could be adjusted from a burst to sustained release profile (Fig. 1B). BMP-2 was 100% encapsulated in microspheres, 50% encapsulated in microspheres, and 50% adsorbed on the hydrogel or 100% adsorbed on the hydrogel.

The three different charge modifications (-OPF: neutral, unmodified; n-OPF: negative, SMA crosslinked; and p-OPF: positive, MAE crosslinked) and three loading methods (Msp: 100% microsphere loading, Cmb: combination of 50% microsphere and 50% adsorption loading, and Ads: 100% adsorption loading) resulted in nine different composites (Fig. 1D). For every charge modification, an implant without BMP-2 loading was included (controls), resulting in a total of 12 different composites. The effect of composite charge and BMP-2 incorporation methods on BMP-2 release was evaluated *in vitro* and *in vivo* by using BMP-2 radiolabeled with ^{125}I. The *in vivo* bioactivity of the released BMP-2 was investigated by analyzing bone formation after 9 weeks of subcutaneous implantation in rats.

BMP-2 radio iodination

Carrier-free $Na^{125}I$ was obtained from PerkinElmer life and Analytical Sciences (Boston, MA). To study the release profiles of BMP-2, a fraction of the incorporated BMP-2 was radiolabeled with ^{125}I, using the chloramine-T method as previously described.[31] The radiolabeled BMP-2 was separated from the free ^{125}I by 24-h dialysis (10 kDa molecular-weight cutoff (MWCO); SpectraPor 7, Rancho Dominguez, CA) against 0.01 M phosphate-buffered saline (PBS) at pH 7.4 (Sigma-Aldrich). The ^{125}I-BMP-2 dialysate was concentrated in a Millipore device (10 kDa; MWCO, Billerica, MA) and the purity was determined by trichloroacetic acid precipitation. The final ^{125}I-BMP-2 preparation contained 99.7% precipitable counts, which indicated the percentage of covalently bound ^{125}I to the BMP-2. Thereafter, ^{125}I-BMP-2 was mixed with nonlabeled BMP-2 (1:5.3 hot:cold ratio) and

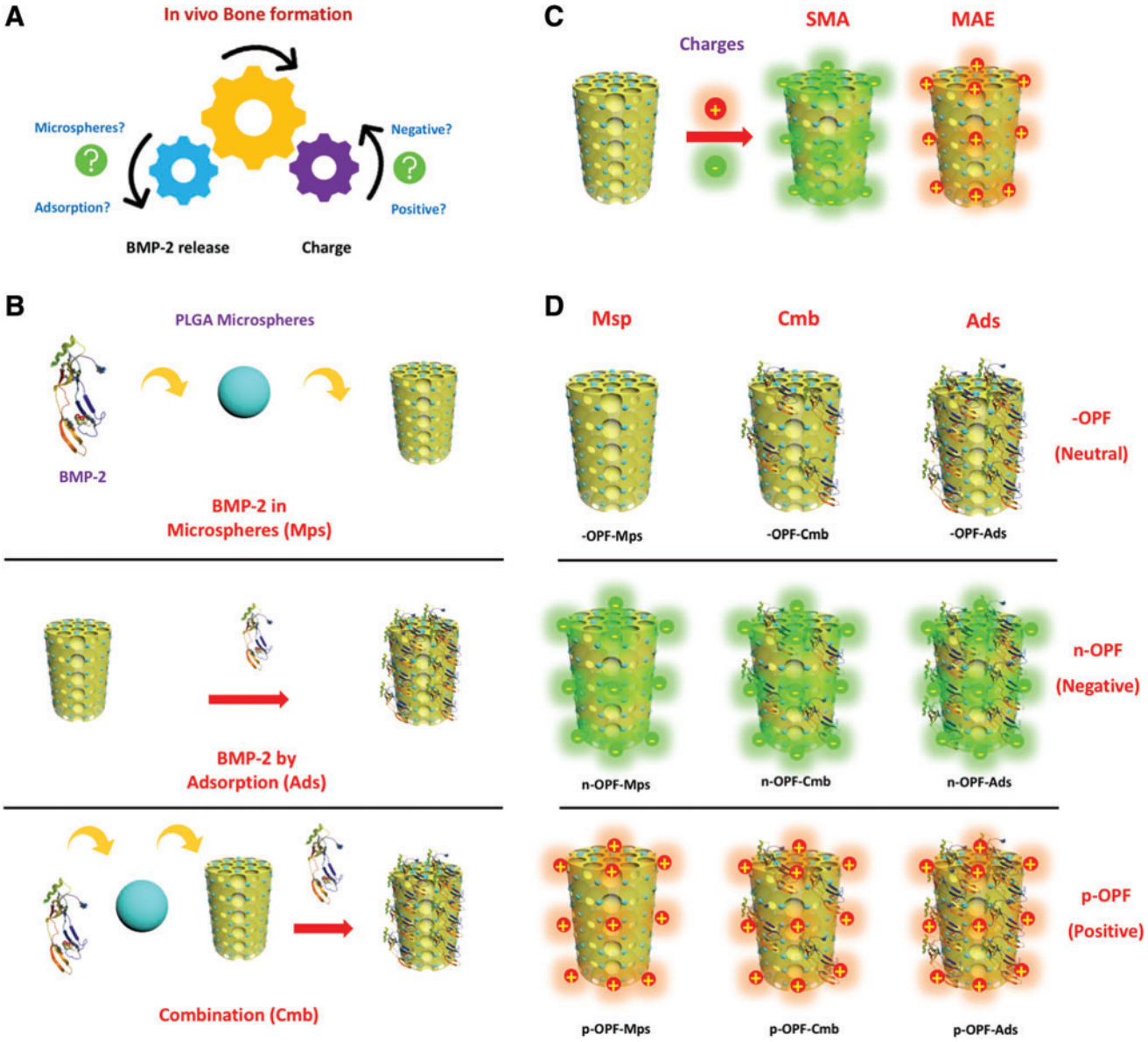

FIG. 1. Schematic design of **(A)** mechanism research question, **(B)** BMP-2 loading methods, **(C)** OPF charge modifications, and **(D)** all OPF formulations. BMP-2, bone morphogenetic protein-2; MAE, -(methacryloyloxy) ethyl)-trimethyl ammonium chloride; SMA, sodium methacrylate; OPF, oligo[(polyethylene glycol) fumarate]; PLGA, poly(lactic-co-glycolic acid); -OPF, unmodified OPF, n-OPF, negatively charged OPF, SMA crosslinked, p-OPF, positively charged OPF, MAE crosslinked. Color images are available online.

incorporated into the composite formulations. A previous study of our group showed biologically active ^{125}I-BMP-2 after labeling using a similar technique.[32]

Microsphere fabrication

PLGA with a lactic to glycolic ratio of 50:50 (M_w 52 kDa; Lakeshore Biomaterials, AL) was used to fabricate microspheres using water-in-oil-in-water (W1-O-W2) double emulsion solvent extraction technique, according to a previously described method.[33] Briefly 0, 50, or 100 µL of 3.7 mg/mL BMP-2-^{125}I-BMP-2 solution was emulsified with 250 mg PLGA 50:50 dissolved in 1.25 mL of dichloromethane using a vortex at 3050 rpm, to obtain 0%, 50%, or 100% BMP-2 loading into microspheres, respectively. The solution was re-emulsified in 2 mL of 2% (w/v) aqueous poly(vinyl alcohol) (PVA, 87–89% mole hydrolyzed, Mw = 13,000–23,000; Sigma-Aldrich) to create the double emulsion and added to 100 mL of a 0.3% (w/v) PVA solution and 100 mL of a 2% (w/v) aqueous isopropanol solution. After 1 h of slowly stirring, the PLGA microspheres were collected by centrifugation at 2500 rpm for 3 min, washed three times with distilled deionized water (ddH_2O), and freeze-dried to a free-flowing powder. After freeze-drying, the morphology of the microspheres was observed by electron microscopy (SEM; S-4700, Hitachi Instruments, Tokyo, Japan) at 5.0 kV. The PLGA microspheres used in this study lose ~80% of their mass within 4 weeks after implantation.[34]

Fabrication of composites

OPF was synthesized using polyethylene glycol with an initial molecular weight of 10 kDa according to previously describes method.[28] OPF (44.4% w/w), N-vinyl pyrrolidone (NVP; 13.3% w/w Sigma-Aldrich St. Louis, MO), Irgacure 2959 (0.2% w/w; Ciba-Specialty Chemicals, Tarrytown, NY), and H_2O (42.1% w/w) solution was mixed with SMA (200 mg, 8.2% w/w, Sigma-Aldrich St. Louis, MO), MAE (225 mg, 10.3% w/w; Sigma-Aldrich St. Louis, MO), or no additive to create hydrogels with a fixed negative (n-OPF), positive (p-OPF), or neutral charge (-OPF), respectively. To create the composites, the OPF/NVP/SMA, OPF/NVP/MAE, or OPF/NVP paste (22.5% w/w) was mixed with NaCl salt particles (75% w/w, sieved to a maximum size of 300 μm) and PLGA microspheres (2.5% w/w).

The resulting mixture was forced into a cylindrical mold with a diameter of 3.5 mm and exposed to UV light (365 nm at intensity of $\sim 8\,mW/cm^2$ black-Ray Model 100AP, Upland, CA) to crosslink the composites for 40 min in total. The composite implants were cut into 6-mm-long rods and immersed in sterile ddH_2O water to leach out the salt. After blot drying, additional BMP-2 was absorbed into certain composite matrices accordingly to the experimental design. To analyze the morphological features of the OPF hydrogels, dry (directly after crosslinking) and hydrated samples were freeze-dried and observed by scanning electron microscopy (SEM) at 5 kV.

The biomaterial characteristics, including surface chemistry, mechanical properties, swelling ratio, zeta potential, and conductivity, were investigated in a previous study.[28] The zeta potential of the used OPF modifications in this study is -1.75 ± 0.7 mV, -5.44 ± 0.6 mV, and 3.7 ± 1.1 mV for -OPF, n-OPF, and p-OPF, respectively. The bioactivity of the released BMP-2 was reported previously and showed a similar bioactivity of the microsphere-encapsulated and hydrogel-adsorbed growth factor after 9 weeks of release.[30] Also, the released BMP-2 generated a similar biologic response compared with freshly added BMP-2 of corresponding dose *in vitro*. The degradation rate of the OPF hydrogel is reported previously and showed minimal *in vitro* degradation of crosslinked hydrogels with an OPF:NVP ratio >0.3 after 21 days in PBS.[35] Furthermore, histology showed a still visible porous structure of OPF after 9 weeks of implantation, as opposed to a fully resorbed Infuse® absorbable collagen sponge (Medtronic, Minneapolis, MN).[30]

In vitro *BMP-2 release*

The *in vitro* release of BMP-2 was analyzed as previously described.[32] Briefly, composite implants placed in a 12-well transwell culture system were exposed to consecutive 7-day W20–17 cell line cultures in Dulbecco's modified Eagle's medium/nutrient mixture F-12 Ham 1:1 mixture (DMEM/F12, Sigma-Aldrich) supplemented with 10% fetal bovine serum and 1% penicillin. The W20 clone 17 cell line is a mouse bone stromal line, known to respond to BMP-2 with an increase in alkaline phosphatase activity.[36] The transwell was transferred into a new culture after 7 days and the medium was analyzed for radiolabeled ^{125}I-BMP using a gamma counter. After 9 weeks, the scaffolds were collected to determine the remaining activity. The ^{125}I activity was corrected for decay and normalized to the starting amount. To analyze the *in vitro* BMP-2 release, the counts/min were correlated to the amount of released BMP-2.

Animals and surgical procedure

Thirty 12-week-old male Harlan Sprague Dawley rats were used for this study according to an approved protocol by the local Animal Care and Use Committee.

Surgery was performed under sterile conditions and general anesthesia (45/10 mg/kg ketamine/xylazine). After shaving and disinfecting the surgical sites, four subcutaneous pockets were created in each limb and filled with ^{125}I-BMP-2-labeled implants. Two subcutaneous pockets in the thoracolumbar region were used to implant the controls (implants without BMP-2 loading). A total of six implants were used per rat with a total of ~ 16 μg BMP-2 per rat. The implants were randomized for application site using a randomized block design per charge modification. Acetaminophen (160 mg in 5 mL added to one pint water bottle) was given as postoperative analgesia for the duration of 1 week. Fluorochrome markers calcein green (10 mg/kg, intraperitoneal) and tetracycline (10 mg/kg, intraperitoneal) were administered at 3 and 6 weeks postoperative, respectively. After 9 weeks, the rats were euthanized by CO_2 asphyxiation to collect the implants for assessment of bone formation by microcomputed tomography (μCT) and subsequent histological analysis.

In vivo *BMP-2 release*

Four scintillation probes connected to digital scalers, as described previously,[33] were used for noninvasive determination of *in vivo* ^{125}I-BMP-2 release kinetics. Directly after wound closure, the ^{125}I-BMP-2 activity was measured to obtain the starting implanted dose. At each subsequent time point (biweekly the first week, weekly from week 1 onward), the rats were anesthetized using isoflurane (induction 4%, maintenance >1.5%) to measure the local ^{125}I-BMP-2 activity over two 1-min periods with two different detectors. To determine the BMP-2 release, the ^{125}I-BMP-2 measurements were corrected for radioactive decay and background activity. The ^{125}I-BMP-2 activity was normalized to the starting implanted dose to determine the retained ^{125}I-BMP-2 dose and released amounts.

In vivo *bone formation*

μCT was used to measure the total bone volume of all implants, including the negative controls without BMP-2. Ex vivo scanning of the scaffolds was performed using a Scanco μCT 35 scanner (Scanco Medical, Switzerland) at 10 μm resolution. Global thresholding at 57 was applied in *ImageJ* (version 2.0.0) to quantify the bone formation (*BoneJ*, plugin of *ImageJ*) within implants.

Histology

The samples were dehydrated in graded series of ethanol and embedded in methyl methacrylate for qualitative assessment by histology. Sections were stained with Gömöri trichrome staining for evaluation of general tissue response and bone formation.[37] Gömöri trichrome stains bone green, osteoid red, fibrous tissue pink, and fat cells white.

Unstained sections were used for fluorescence imaging of calcein green and tetracycline.

Statistical analysis

Statistical analysis was performed using SPSS 22.0 software (SPPS, Inc., Chicago, IL). *In vitro* ($n=3$) and *in vivo* results ($n=10$) are given as means ± standard deviations (SDs). The 3D μCT reconstructions were shown for the median value of each group. Before the *in vivo* study, power analysis estimated that to demonstrate a relevant difference of at least 20% at an alpha of 0.05 and an SD of 1.4, the groups should be $n=8$ per condition at a power of 80%. All data sets were tested for outliers using residuals, for normality of the residuals using the Shapiro–Wilk test and for homogeneity of variances using the Levene's test. Nonparametric data were analyzed with Kruskal–Wallis and Benjamini–Hochberg *post hoc* tests. Parametric data were analyzed with univariate analysis of variances followed by Benjamini–Hochberg *post hoc* (homogeneous variances) or Games–Howell *post hoc* (unequal variances). Differences were considered significant for $p<0.05$. Based on *in vitro* bioactivity assays, >25 ng BMP-2/mL was considered a biologically relevant difference for *in vitro* BMP-2 release. Differences *in vivo* release BMP-2 were considered clinically relevant at >100 ng BMP-2.[38,39]

Results

BMP-2 labeling and incorporation

Labeling of the BMP-2 with ^{125}I resulted in an activity per mass of 6.1 μCi/μg. The microspheres were loaded with either 2.9 or 1.3 μg BMP-2/mg PLGA. A schematic demonstration of the fabrication of PLGA microspheres is shown in Figure 2A. The composite scaffold characteristics are summarized in Table 1. The different loading methods resulted in comparable BMP-2 loading per scaffold. However, OPF modifications aiming at electrical charge resulted in significant ($p<0.01$) differences in BMP-2 loading within these OPF groups due to differences in loss of BMP-2 during the fabrication process. To correct this, the release kinetics was normalized to the starting amount of BMP-2 loading for each individual composite *in vitro* and *in vivo*. SEM of the PLGA microspheres, performed after freeze-drying, showed a smooth surface similar for unloaded and BMP-2-loaded microspheres (Fig. 2B, C). The diameter of the microspheres varied between 5 and 85 μm. Figure 2D

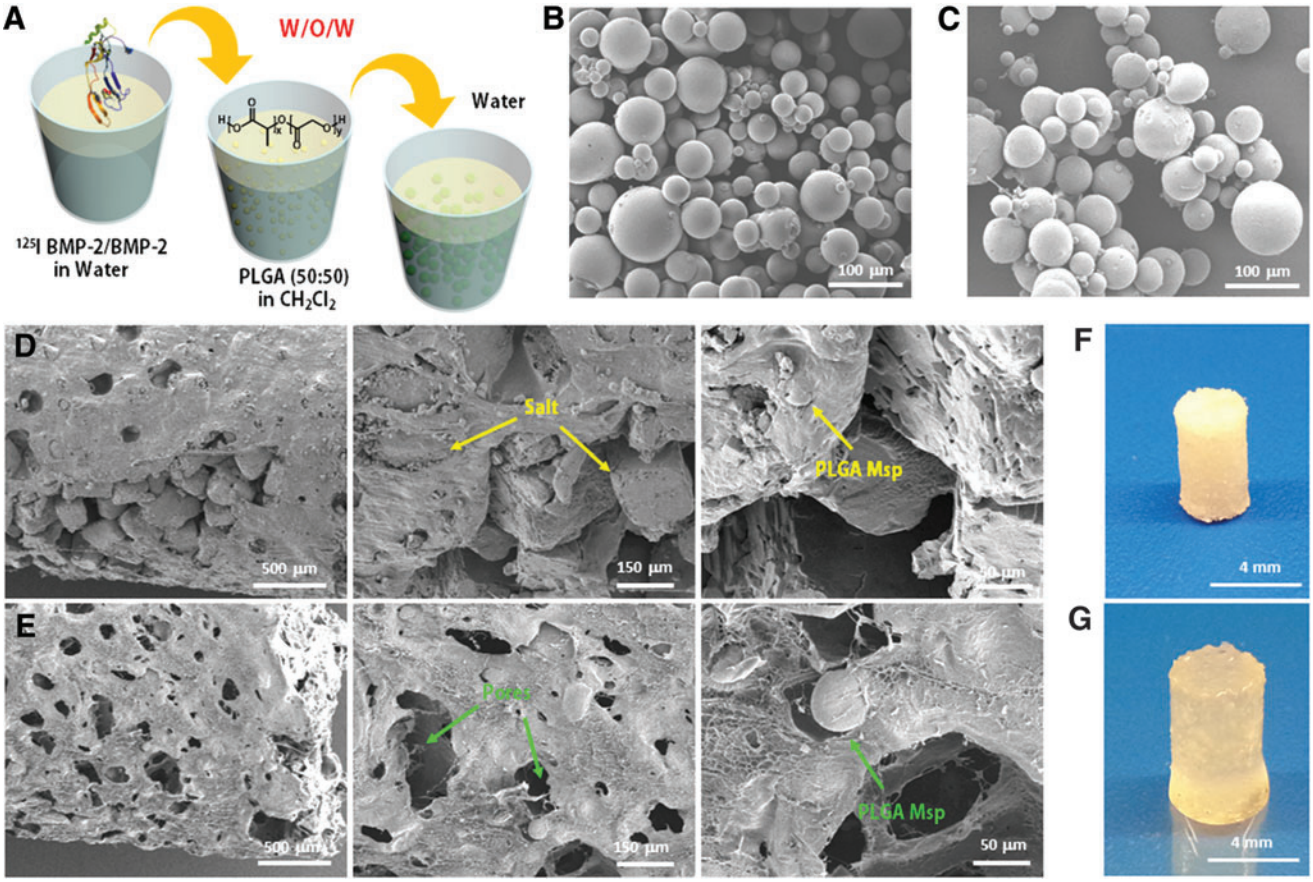

FIG. 2. **(A)** Water-in-oil-in-water (W1-O-W2, W/O/W) fabrication of microspheres. SEM images of **(B)** PLGA microspheres and **(C)** PLGA microspheres loaded with BMP-2. SEM images of OPF hydrogel **(D)** before and **(E)** after the salt leaching process. Photograph of **(F)** dried OPF hydrogel before salt leaching and **(G)** hydrated OPF hydrogel after salt leaching. Msp, microspheres; PLGA, poly(lactic-co-glycolic acid); SEM, scanning electron microscope. Color images are available online.

Table 1. Composite Implant Characteristics

Composite name	BMP-2 loading		Initial activity/implant (μCi)	BMP-2/implant (μg)
	Hydrogel	Microspheres		
-OPF-Msp	0% Adsorbed	100% Loaded	3.66 ± 0.79	4.71 ± 1.02
-OPF-Cmb	50% Adsorbed	50% Loaded	3.48 ± 0.15	4.58 ± 0.2
-OPF-Ads	100% Adsorbed	0% Loaded	3.75 ± 0.2	4.88 ± 0.25
n-OPF-Msp (negative charge)	0% Adsorbed	100% Loaded	2.98 ± 0.45	3.83 ± 0.58
n-OPF-Cmb (negative charge)	50% Adsorbed	50% Loaded	2.71 ± 0.17	3.57 ± 0.22
n-OPF-Ads (negative charge)	100% Adsorbed	0% Loaded	3.04 ± 0.08	3.96 ± 0.11
p-OPF-Msp (positive charge)	0% Adsorbed	100% Loaded	2.37 ± 0.32	3.05 ± 0.41
p-OPF-Cmb (positive charge)	50% Adsorbed	50% Loaded	2.29 ± 0.14	3.01 ± 0.18
p-OPF-Ads (positive charge)	100% Adsorbed	0% Loaded	2.48 ± 0.12	3.23 ± 0.16

Msp, 100% BMP-2 loaded in PLGA microspheres; Cmb, 50% BMP-2 loaded in PLGA microspheres, 50% BMP-2 adsorbed on the hydrogel; Ads, 100% BMP-2 loaded on the hydrogel; -OPF, unmodified OPF; n-OPF, negatively charged OPF; p-OPF, positively charged OPF.

BMP-2, bone morphogenetic protein-2; Msp, microspheres; OPF, oligo[(polyethylene glycol) fumarate]; PLGA, poly(lactic-co-glycolic acid).

shows SEM images of the hydrogels before salt leaching, with microspheres and salt particles embedded in the hydrogel matrix. Salt leaching resulted in randomly distributed microporous hydrogels with the microspheres embedded in the hydrogel matrix (Fig. 2E). Typical hydrogels before and after salt leaching are shown in Figure 2F and G, respectively.

In vitro *release kinetics*

Effect of charge modification. For the % BMP-2 release per time point, the OPF charge modifications affected the *in vitro* BMP-2 release overall significantly. Whereas -OPF composites released significantly ($p < 0.01$) more BMP-2 compared with n-OPF and p-OPF, p-OPF released significantly ($p < 0.01$) less compared with n-OPF within 3 days. Subsequently, n-OPF released more ($p < 0.01$) BMP-2 compared with -OPF and p-OPF from week 2 to 6, while p-OPF released less ($p < 0.01$) BMP-2 compared with -OPF and n-OPF from week 3 to 6. Corresponding overall cumulative release profiles are shown in Figure 3A.

Post hoc analysis of charge modifications showed significant differences within OPF-Msp, OPF-Cmb, and OPF-Ads groups. For OPF-Msp composites with a more sustained release profile, -OPF-Msp released significantly ($p < 0.02$, week 0.5 (W0.5): 27.5% ± 2.0%, W1: 11.6% ± 1.0%) more BMP-2 compared with n-OPF-Msp (W0.5: 11.0% ± 1.1%, W1: 8.6% ± 1.3%) and p-OPF-Msp (W0.5: 16.5% ± 2.1%, W1: 8.3% ± 0.7%) composites during the first week. Whereas n-OPF-Msp released more ($p < 0.01$) BMP-2 compared with -OPF-Msp and p-OPF-Msp, p-OPF-Msp released less ($p < 0.01$) compared with -OPF-Msp at 3 and 4 weeks. Corresponding OPF-Msp cumulative release profiles are shown in Figure 3B.

For OPF-Cmb composites with a combination of burst and sustained release profile, n-OPF-Cmb showed a lower ($p < 0.03$, 20.9% ± 1.9%) BMP-2 burst release compared with -OPF-Cmb (33.6% ± 5.2%) and p-OPF-Cmb (28.1% ± 2.3%) composites after 3 days. Whereas n-OPF-Cmb released more ($p < 0.01$) BMP-2 compared with -OPF-Cmb and p-OPF-Cmb, p-OPF-Cmb released less ($p < 0.01$) compared with -OPF-Cmb at 3 and 4 weeks. Furthermore, n-OPF-Cmb released significantly ($p < 0.006$) more BMP-2 compared with p-OPF-Cmb at 2 and 5 weeks. For the remaining period, p-OPF-Cmb released less ($p < 0.006$) BMP-2 during week 6 and 7 and more BMP-2 during week 8 and 9 compared with the other OPF-Cmb composites. The corresponding cumulative release profiles for OPF-Cmb composites are shown in Figure 3C.

For OPF-Ads composites, with a larger burst release, n-OPF-Ads showed a significantly smaller BMP-2 burst release ($p < 0.01$, 32.4% ± 5.3%) compared with the other -OPF-Ads (49.2% ± 4.9%) and p-OPF-Ads (49.1% ± 3.7%) composites after 3 days. Subsequently, p-OPF-Ads released more ($p < 0.01$) BMP-2 compared with -OPF-Ads and n-OPF-Ads at 1 week. From week 2 onward, n-OPF-Ads released significantly ($p < 0.02$) more BMP-2 compared with the other OPF-Ads composites. p-OPF-Ads released significantly ($p < 0.04$) less BMP-2 compared with the other OPF-Ads composites at 4 and 5 weeks. The corresponding cumulative release profiles for OPF-Ads composites are shown in Figure 3D.

Effect of loading method. Overall, the BMP-2 loading method significantly affected the *in vitro* growth factor release. OPF-Msp released significantly ($p < 0.05$) less BMP-2 compared with OPF-Cmb and OPF-Ads until week 3, while OPF-Ads released significantly ($p < 0.01$) more BMP-2 compared with OPF-Cmb. For the remaining period, OPF-Msp and OPF-Cmb released significantly ($p < 0.01$) more BMP-2 compared with OPF-Ads. The corresponding overall cumulative release profiles are shown in Figure 3E.

Post hoc analysis of the loading effects showed significant differences within the -OPF, n-OPF, and p-OPF groups. For the -OPF composites, within the first 3 days BMP-2 burst release was significantly ($p < 0.05$) different between -OPF-Msp (27.5% ± 2.0%), -OPF-Cmb (33.6% ± 5.2%), and -OPF-Ads (49.2% ± 4.9%). Whereas -OPF-Ads released significantly ($p < 0.05$) more BMP-2 compared with the other -OPF composites until week 2, -OPF-Msp and -OPF-Cmb release rates were significantly ($p < 0.01$) higher compared with -OPF-Ads from week 5 onward. The corresponding -OPF cumulative release profiles are shown in Figure 3F.

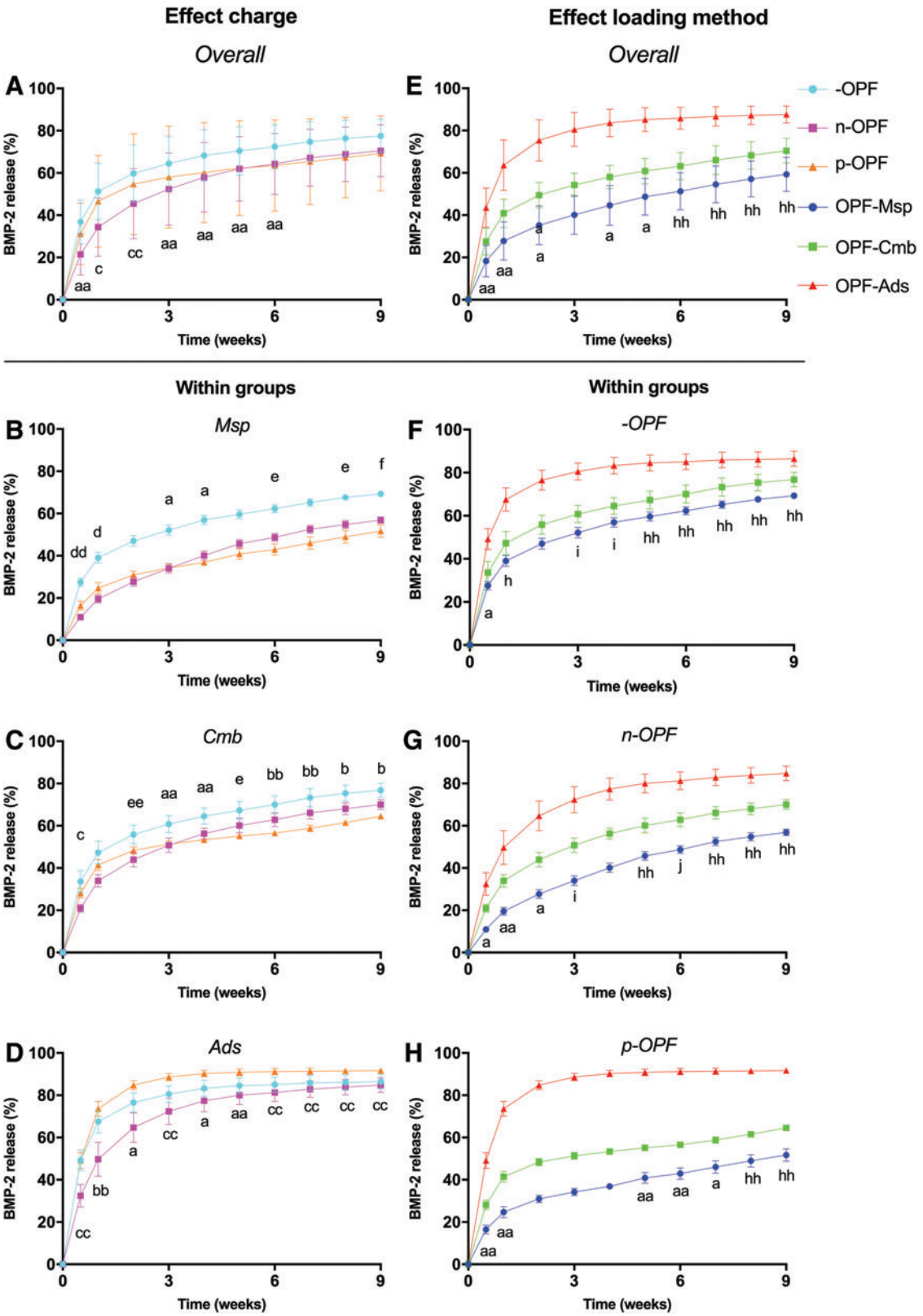

FIG. 3. The effect of charge modifications **(A–D)** and BMP-2 loading method **(E–H)** in OPF hydrogels on ^{125}I-BMP-2 release kinetics, shown in % cumulative BMP-2 release. Graphs represent the overall effect **(A, E)** and effect within groups **(B–D and F–H)**. *One letter* indicates a significant difference at $p < 0.05$, and *two letters* indicate a significant difference at $p < 0.01$. Significantly different BMP-2 release is indicated between a: all formulations, b: p-OPF versus -OPF and n-OPF, c: n-OPF versus -OPF and p-OPF, d: -OPF versus n-OPF and p-OPF, e: n-OPF versus p-OPF, f: -OPF versus p-OPF, h: OPF-Ads versus OPF-Cmb and OPF-Msp, i: OPF-Ads versus OPF-Msp, j: OPF-Cmb versus OPF-Ads. OPF, oligo[(polyethylene glycol) fumarate]; Msp, 100% BMP-2 loaded in PLGA microspheres; Cmb, 50% BMP-2 loaded in PLGA microspheres, 50% BMP-2 adsorbed on the hydrogel; Ads, 100% BMP-2 loaded on the hydrogel; -OPF, unmodified OPF; n-OPF, negatively charged OPF; p-OPF, positively charged OPF. Color images are available online.

For n-OPF composites, n-OPF-Msp released the least ($p < 0.45$; W0.5: 11.0% ± 1.1%, W1: 8.0% ± 1.3%, W2: 8.2% ± 1.1%) and n-OPF-Ads released the most ($p < 0.01$; W0.5: 32.4% ± 5.3%, W1: 17.3% ± 2.7%, W2: 15.0% ± 1.2%) BMP-2 during the first 2 weeks. n-OPF-Msp and n-OPF-Cmb released significantly ($p < 0.01$) more BMP-2 compared with n-OPF-Ads at 6, 8, and 9 weeks. For the n-OPF composites, the corresponding cumulative release profiles are shown in Figure 3G.

For the p-OPF composites, p-OPF-Msp released the least BMP-2 ($p < 0.01$; W0.5: 16.5% ± 2.1%, W1: 8.3% ± 0.7%) and p-OPF-Ads the most ($p < 0.01$; W0.5: 49.1% ± 3.7%, W1: 24.5% ± 0.7%) during the first week. BMP-2 release from p-OPF-Msp and p-OPF-Cmb was significantly ($p < 0.01$) higher compared with p-OPF-Ads from week 5 to 9. The corresponding cumulative release profiles are shown in Figure 3H.

Animals

Five rats died one day after surgery, probably due to oversensitivity to xylazine, since no health problems were observed in the remainder of the rats after xylazine was lowered. Eight implants were removed by the rats from the subcutaneous pocket during the follow-up and were lost. This resulted in group sizes of p-OPF-Msp $n = 10$; p-OPF-Cmb and p-OPF-Ads $n = 9$; -OPF-Msp and -OPF-Cmb $n = 8$; -OPF-Ads, n-OPF-Cmb, and n-OPF-Ads $n = 6$; and n-OPF-Msp $n = 5$. No BMP-2 unloaded controls were removed during follow-up.

In vivo *BMP-2 release*

Effect of charge modification. Overall, charge modifications affected the *in vivo* BMP-2 release significantly. p-OPF showed a significantly ($p < 0.01$) smaller burst release compared with -OPF and n-OPF within 3 days. Subsequently, p-OPF released more ($p < 0.02$) compared with the other composites at week 4 and 5. The corresponding cumulative overall release profiles are shown in Figure 4A.

Post hoc analysis of the charge modifications showed significant differences in OPF-Msp, OPF-Cmb, and OPF-Ads groups. For OPF-Msp with a more sustained release profile of BMP-2, p-OPF-Msp released significantly ($p < 0.01$, 33.6% ± 7.4%) less BMP-2 compared with -OPF-Msp (52.1% ± 6.1%) and n-OPF-Msp (46.4% ± 6.9%) within 3 days, while releasing more ($p < 0.009$) at 4 and 5 weeks. Furthermore, n-OPF-Msp released more ($p < 0.03$) BMP-2 compared with p-OPF-Msp at week 2. For OPF-Msp composites, the corresponding cumulative release profiles are shown in Figure 4B.

In OPF-Cmb composites with a combination of burst and sustained release profile, p-OPF-Cmb released the least ($p < 0.01$, 42.5% ± 4.7%) BMP-2 and -OPF-Cmb the most ($p < 0.01$, 65.2% ± 2.6%) BMP-2 within 3 days. n-OPF-Cmb released significantly ($p < 0.04$) more BMP-2 compared with both OPF-Cmb composites at week 2 and compared with -OPF-Cmb at week 3. Subsequently, p-OPF-Cmb released more ($p < 0.01$) BMP-2 compared with the other OPF-Cmb composites at week 4 and 5. The corresponding cumulative release profiles for OPF-Cmb composites are shown in Figure 4C.

For OPF-Ads composites with a burst release profile, p-OPF-Ads showed a significantly ($p < 0.01$, 78.9% ± 5.5%) smaller burst release compared with n-OPF-Ads (81.4% ± 3.6%) within 3 days. Subsequently, p-OPF-Ads released more ($p < 0.03$) BMP-2 compared with the other OPF-Ads composites at week 1. The corresponding OPF-Ads cumulative release profiles are shown in Figure 4D.

Effect of loading method. Overall, the BMP-2 loading method influenced the *in vivo* growth factor release significantly in a similar trend as *in vitro*. Whereas OPF-Msp released less ($p < 0.01$) BMP-2 compared with OPF-Cmb and OPF-Ads, OPF-Ads released more ($p < 0.01$) BMP-2 compared with OPF-Cmb within 3 days. From week 2 to 5, OPF-Msp and OPF-Cmb released significantly ($p < 0.01$) more BMP-2 compared with OPF-Ads. OPF-Ads released significantly ($p < 0.01$) less BMP-2 compared with OPF-Msp and OPF-Cmb from week 2 to 4. The corresponding overall cumulative release profiles are shown in Figure 4E.

Post hoc analysis of loading methods showed significant differences in OPF-Msp, OPF-Cmb, and OPF-Ads groups. In -OPF, -OPF-Msp released the least ($p < 0.03$, 52.1% ± 6.1%) BMP-2 and -OPF-Ads released the most ($p < 0.01$, 81.4% ± 3.6%) BMP-2 at 3 days, 2 weeks, and 3 weeks. -OPF-Msp and -OPF-Cmb released more ($p < 0.03$) BMP-2 compared with -OPF-Ads at 4 and 5 weeks. For the -OPF composites, the corresponding cumulative release profiles are shown in Figure 4F.

For n-OPF, significant different burst releases were seen with n-OPF-Msp releasing the least ($p < 0.01$, 46.4% ± 6.9%) and n-OPF-Ads releasing the most ($p < 0.01$, 86.7% ± 5.2%) BMP-2 within 3 days. n-OPF-Msp and n-OPF-Cmb released more ($p < 0.04$) BMP-2 compared with n-OPF-Ads from week 1 to 5. The corresponding cumulative release profiles for n-OPF composites are shown in Figure 4G.

For p-OPF, significantly different burst releases were seen with p-OPF-Msp releasing the least ($p < 0.01$, 33.6% ± 7.4%) and p-OPF-Ads releasing the most ($p < 0.01$, 78.9% ± 5.5%) within 3 days. p-OPF-Msp and p-OPF-Cmb released significantly more ($p < 0.03$) BMP-2 compared with p-OPF-Ads from week 2 to 5 and at week 7. The corresponding p-OPF cumulative release profiles are shown in Figure 4H.

μCT analysis

In all unloaded implants (not containing BMP-2), no bone formation was observed. Overall, n-OPF (48.4 ± 47.2 mm^3) showed significant ($p < 0.001$) greater bone formation compared with -OPF (10.5 ± 20.8 mm^3) and p-OPF (4.9 ± 15.8 mm^3; Fig. 5A). Also in individual groups with different BMP-2 loading methods and subsequent release profiles, n-OPF contained significantly ($p < 0.05$) more bone volume compared with the -OPF and p-OPF groups (OPF-Msp group: n-OPF 48.4 ± 47.1 mm^3, -OPF 12.3 ± 18.5 mm^3, and p-OPF 10.1 ± 25.6 mm^3; OPF-Cmb group: n-OPF 56.3 ± 43.6 mm^3, -OPF 15.9 ± 28.9 mm^3, and p-OPF 3.8 ± 6.6 mm^3; and OPF-Ads group: n-OPF 40.5 ± 57.5 mm^3, -OPF 0.8 ± 1.8 mm^3, and p-OPF 0.06 ± 0.09 mm^3; Fig. 5B). Normalizing bone formation by released BMP-2 ($mm^3/\mu g$) showed similar results (Supplementary Fig. S1).

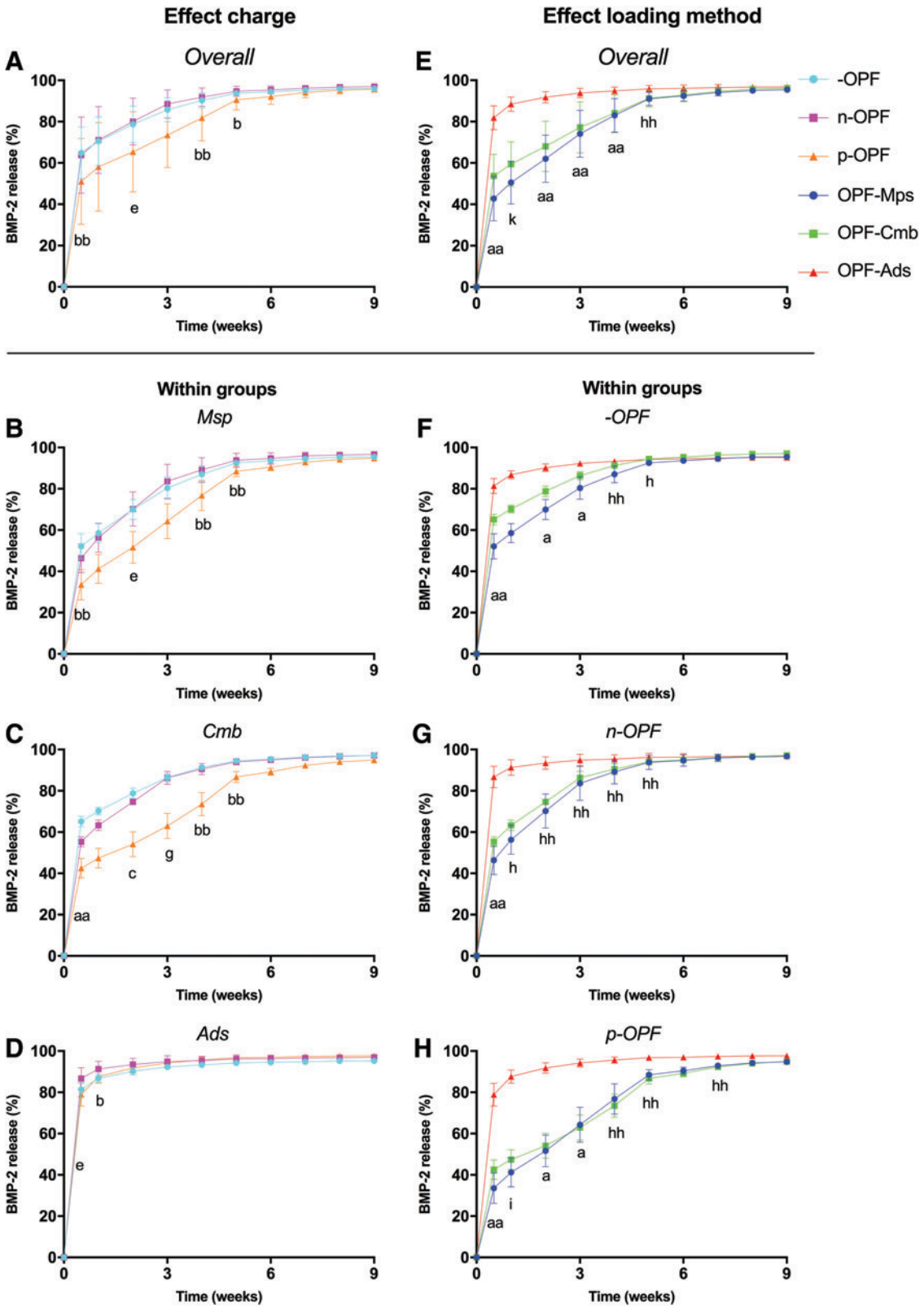

FIG. 4. The effect of charge modifications **(A–D)** and BMP-2 loading method **(E–H)** in OPF hydrogels on ^{125}I-BMP-2 release kinetics *in vivo*, shown in % cumulative BMP-2 release. Graphs represent the overall effect **(A, E)** and effect within groups **(B–D and F–H)**. *One letter* indicates a significant difference at $p < 0.05$, and *two letters* indicate a significant difference at $p < 0.01$. Significantly different BMP-2 release is indicated between a: all formulations, b: p-OPF versus -OPF and n-OPF, c: n-OPF versus -OPF and p-OPF, d: -OPF versus n-OPF and p-OPF, e: n-OPF versus p-OPF, f: -OPF versus p-OPF, h: OPF-Ads versus OPF-Cmb and OPF-Msp, i: OPF-Ads versus OPF-Msp, j: OPF-Cmb versus OPF-Ads. OPF, oligo[(polyethylene glycol) fumarate]; Msp, 100% BMP-2 loaded in PLGA microspheres; Cmb, 50% BMP-2 loaded in PLGA microspheres, 50% BMP-2 adsorbed on the hydrogel; Ads, 100% BMP-2 loaded on the hydrogel; -OPF, unmodified OPF; n-OPF, negatively charged OPF; p-OPF, positively charged OPF. Color images are available online.

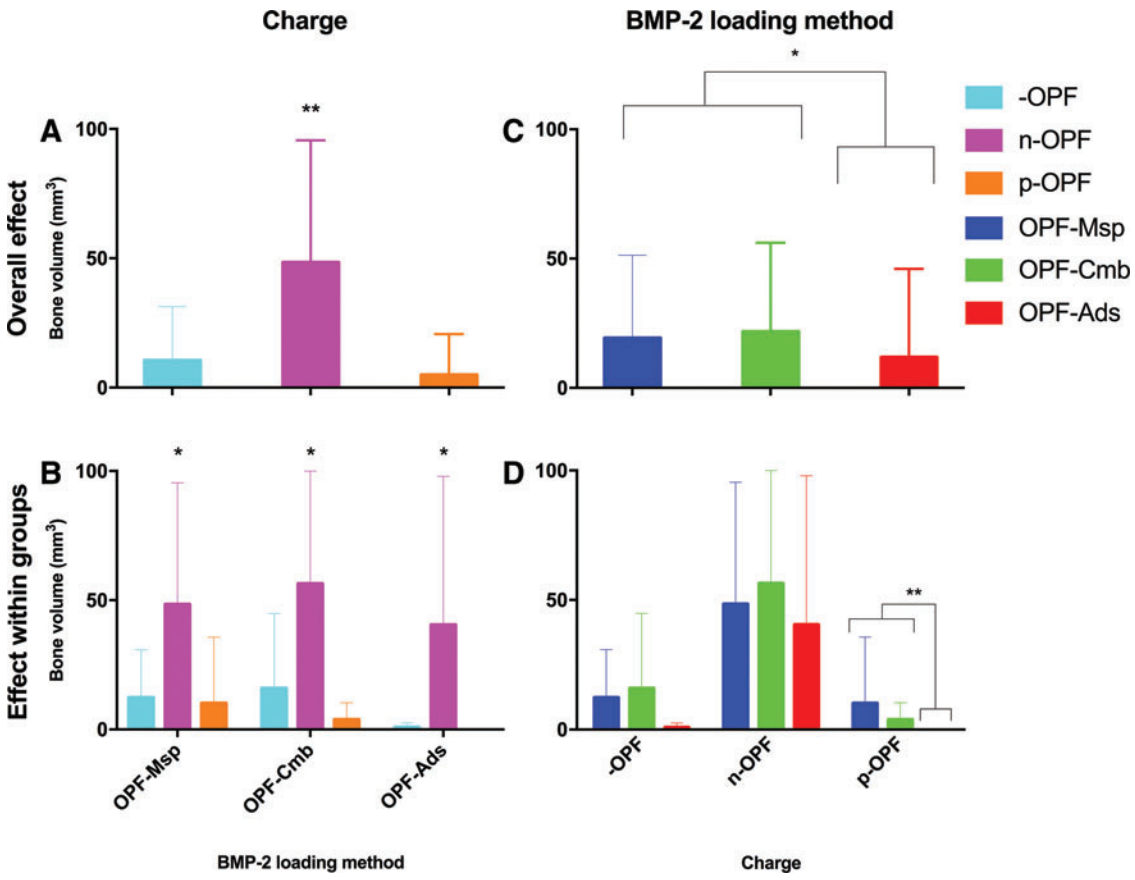

FIG. 5. Amount of newly formed bone after 9 weeks of subcutaneous implantation, shown in total bone volume (mm^3). Data represent the overall effect of OPF charge modifications **(A)**, the effect within BMP-2 loading methods **(B)**, the overall effect of BMP-2 loading method **(C)**, and the effect within OPF charge modifications **(D)**. *One symbol* (*) indicates a significant difference with $p < 0.05$, and *two symbols* (**) indicate a significant difference with $p < 0.01$ versus all other implants within the groups unless specifically indicated otherwise. Msp, 100% BMP-2 loaded in PLGA microspheres; Cmb, 50% BMP-2 loaded in PLGA microspheres, 50% BMP-2 adsorbed on the hydrogel; Ads, 100% BMP-2 loaded on the hydrogel; -OPF, unmodified OPF; n-OPF, negatively charged OPF; p-OPF, positively charged OPF. Color images are available online.

Fully or partially loading BMP-2 in microspheres showed a significant ($p < 0.04$) increase in bone formation compared with fully adsorbing the BMP-2 on the composite (OPF-Msp $19.2 \pm 32.1\,mm^3$, OPF-Cmb $21.7 \pm 34.4\,mm^3$, OPF-Ads $11.8 \pm 34.2\,mm^3$; Fig. 5C). Within OPF charge modifications, this trend was observed for p-OPF, with p-OPF-Msp and p-OPF-Cmb showing significantly ($p < 0.008$) more bone formation compared with p-OPF-Ads (Fig. 5D). No significant effect of microsphere loading was seen within -OPF and n-OPF.

The 3D reconstructions confirm these data, showing diffuse bone formation in the pores of n-OPF (Fig. 6D–F) and minimal bone formation in -OPF (Fig. 6A–C) and p-OPF (Fig. 6G–I).

Histology

In -OPF, histological analysis showed minimal fibrous tissue ingrowth in the unloaded negative controls (Fig. 7A, E). No bone formation and a mild inflammatory response were observed in these composites. -OPF-Msp showed ingrowth mainly consisting of fibrous tissue, osteoid, and woven bone with a minimal inflammatory response (Fig. 7B, F). More tissue ingrowth was seen in -OPF-Cmb showing a similar inflammatory response and tissue ingrowth as -OPF-Msp (Fig. 7C, G). In -OPF-Ads, minimal fibrous tissue in growth was seen with a minimal inflammatory response (Fig. 7D, H).

In n-OPF, the unloaded controls showed no bone formation with mainly ingrowth of fibrous tissue and a moderate inflammatory response (Fig. 7I, M). n-OPF-Msp showed tissue ingrowth of woven bone, fat cells, and fibrous tissue with a mild inflammatory response (Fig. 7J, N). The bone was formed on the scaffold surface with fat cells centrally in the pores. Also, n-OPF-Cmb showed ingrowth of woven bone on the surface of the scaffold with fat cells, fibrous tissue, and a minimal inflammatory response (Fig. 7 K, O). In n-OPF-Ads, tissue ingrowth was typed as a combination of osteoid, bone, fat cells, and fibrous tissue accompanied with a minimal inflammatory response (Fig. 7L, P). The bone was seen in good contact with the scaffold and fat cells centrally in the pores.

In the p-OPF, the unloaded control showed no bone formation, with minimal fibrous tissue ingrowth and a mild

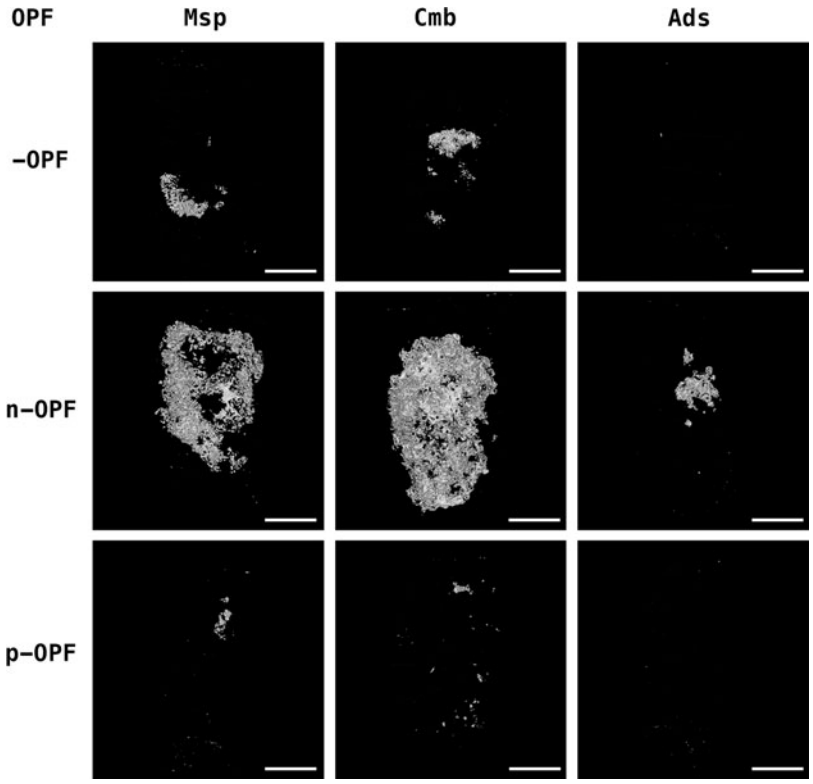

FIG. 6. Representative 3D μCT reconstructions of the BMP-2 containing implants after 9 weeks of subcutaneous implantation. Msp, 100% BMP-2 loaded in PLGA microspheres; Cmb, 50% BMP-2 loaded in PLGA microspheres, 50% BMP-2 adsorbed on the hydrogel; Ads, 100% BMP-2 loaded on the hydrogel; -OPF, unmodified OPF; n-OPF, negatively charged OPF; p-OPF, positively charged OPF. Scale bars represent 1000 μm. 3D, three dimensional; μCT, microcomputed tomography.

inflammatory response (Fig. 7Q, U). All BMP-2-loaded p-OPF showed similar minimal tissue ingrowth consisting mainly of fibrous tissue and very minimal osteoid with calcifications (Fig. 7R–T, V–X). The inflammatory response was typed as mild for these p-OPF composites.

Fluorescence markers calcein green (green) and tetracycline (orange) showed the aspect of woven (Fig. 8D, E, G, and H) and lamellar (Fig. 8A, B, and F) bone disposition starting at various locations both early (3 weeks, calcein) and late (6 weeks, tetracycline) in the pores of -OPF-Msp, -OPF-Cmb, all n-OPF, p-OPF-Msp, and p-OPF-Cmb hydrogels (Fig. 8A, B, and D–H).

Discussion

Electrical charge modifications of OPF composite scaffold had a significant effect on BMP-2 release and bone formation. For microsphere-encapsulated BMP-2, p-OPF decreased the burst release and released the BMP-2 in a more sustained release manner *in vivo*. Regardless of the BMP-2 loading method, significantly more bone formation was seen in n-OPF compared with neutral and positive charge. Other than electrical charge, the BMP-2 loading methods also affected BMP-2 release and bone formation significantly. Whereas BMP-2 adsorption on the composite matrix mainly resulted in a large burst release with subsequent low-dose sustained release, BMP-2 encapsulation in the microspheres decreased the burst release and resulted in a more sustained release over time. The more sustained BMP-2 release by microsphere encapsulation resulted in significantly more bone formation compared with adsorption alone. All variables that influenced BMP-2 release and bone formation are discussed in detail.

The biomaterial electrical charge influenced BMP-2-induced bone formation

Regardless of the BMP-2 loading method, negatively charged OPF augmented bone formation better than neutral and positively charged OPF. In line with our results, previous studies showed superior mineralization and bone-like cellular attachment *in vitro* and improved bone formation *in vivo* on various negatively charged biomaterials and natural bone.[12,20,25–27,40–45] More recently, multiple studies investigated the underlying mechanism using polarized HAp.[25,26,43,45,46] A suggested theory is that the negatively charged surface has high affinity with Ca^{2+}, which will in turn enhance biomineralization. The biomineralized surface will attract several adhesion molecules that stimulate bone-like cellular attachment to the biomaterial. In line with this, several synthetic polymers showed improved biomineralization, cell adhesion, and cell proliferation when functionalized with anionic functional groups.[47]

Although this showed that electrical charge is an important mechanism driving osteoconduction, it should be taken into account that the biomaterial surface chemistry and physical properties also play a role in this process. The charge modifications of OPF required incorporation of an additional compound and consequently modified the chemical structure of the biomaterial. For biomaterial surface chemistry, it has been shown that apart from anionic functional groups, the cationic amine group is associated with improved biomineralization by strong affinity for phosphate.[48] For biomaterial physical properties, studies investigating polarized HAp have shown that surface roughness could potentially override the effect of surface charge.[49] However, overall, this study and previous research strongly indicate that functionalizing biomaterials with a negative

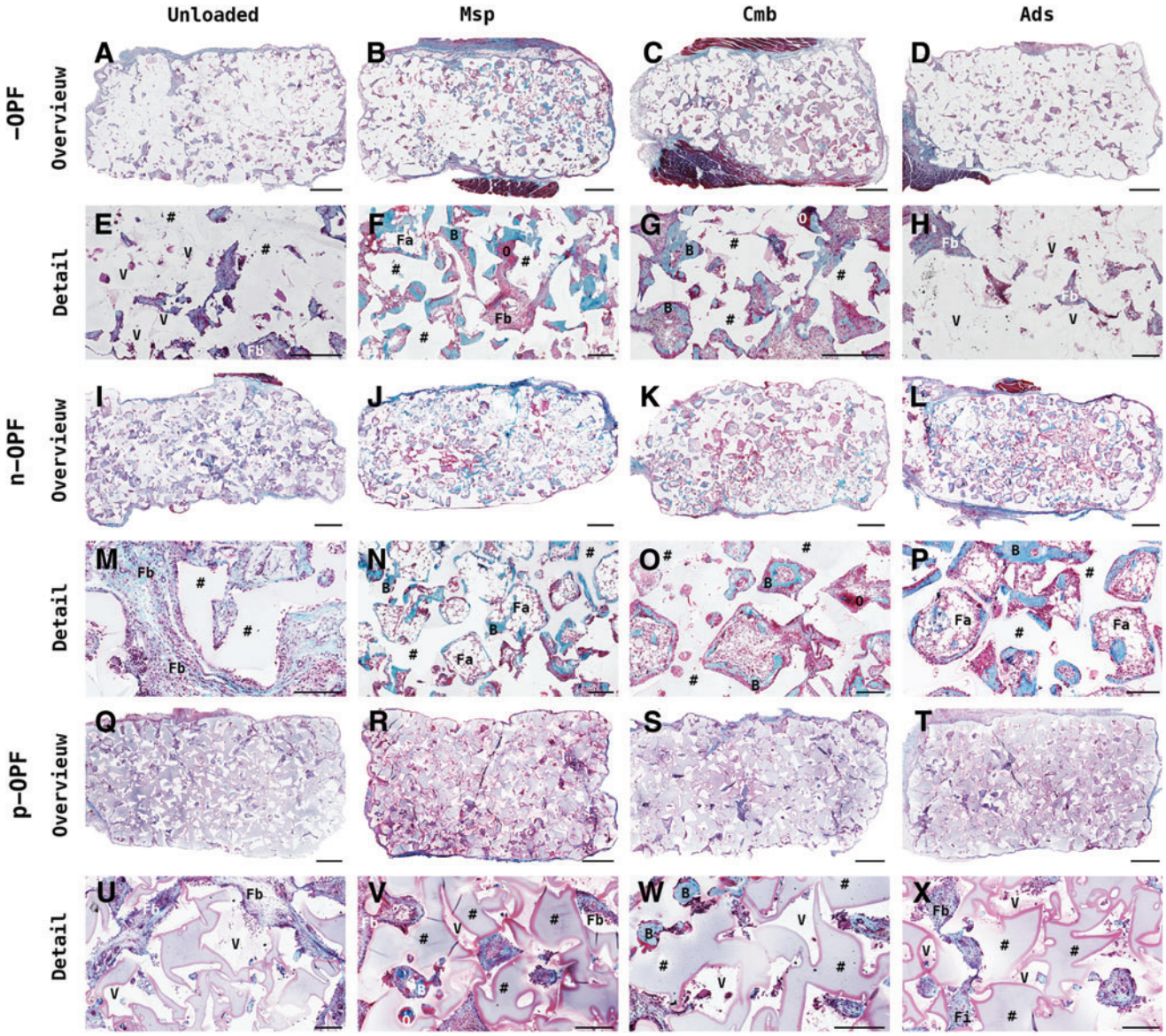

FIG. 7. Gömöri trichrome-stained histological sections of -OPF unloaded **(A, E)**, -OPF-Msp **(B, F)**, -OPF-Cmb **(C, G)**, -OPF-Ads **(D, H)**; n-OPF unloaded **(I, M)**, n-OPF-Msp **(J, N)**, n-OPF-Cmb **(K, O)**, n-OPF-Ads **(L, P)**; and p-OPF unloaded **(Q, U)**, p-OPF-Msp **(R, V)**, p-OPF-Cmb **(S, W)**, p-OPF-Ads **(T, X)** after 9 weeks of subcutaneous implantation. The OPF hydrogels (#) formed an interconnected porous network with fibrous tissue (Fb), fat tissue (Fa), bone (B), and osteoid (O) ingrowth in the BMP-2-loaded composites. Whereas only small bony islands were seen in p-OPF, substantial tissue ingrowth was seen in n-OPF with bone and osteoid growing on the surface of the hydrogel with fat cells centrally in the pores. Much void (V) volume was seen in unloaded -OPF, -OPF-Ads, and all p-OPF composites. Scale bars represent 1000 μm **(A–D, I–L, and Q–T)**, 500 μm **(E, G)**, and 200 μm **(F, H, M–P, and U–X)**. Msp, 100% BMP-2 loaded in PLGA microspheres; Cmb, 50% BMP-2 loaded in PLGA microspheres, 50% BMP-2 adsorbed on the hydrogel; Ads, 100% BMP-2 loaded on the hydrogel; -OPF, unmodified OPF; n-OPF, negatively charged OPF; p-OPF, positively charged OPF. Color images are available online.

surface charge has great potential for bone tissue engineering.

Sustained BMP-2 release by microsphere encapsulation augments bone formation compared with sole adsorption of BMP-2 on the composite

Overall, a BMP-2 burst release ranging from 40% to 52% with subsequent sustained release generated significant more bone in OPF composites compared with composites with >80% of BMP-2 released within 3 days. This highlights that timing of release is an important factor influencing BMP-2-induced bone formation. Although the beneficial effect of local BMP-2 retention by biomaterials on bone formation is evident,[3–5,50] the optimal release rate remains unknown. So far, various BMP-2 release profiles have shown good bone formation in several biomaterials,[3,5,32,51–55] but few studies have explored the

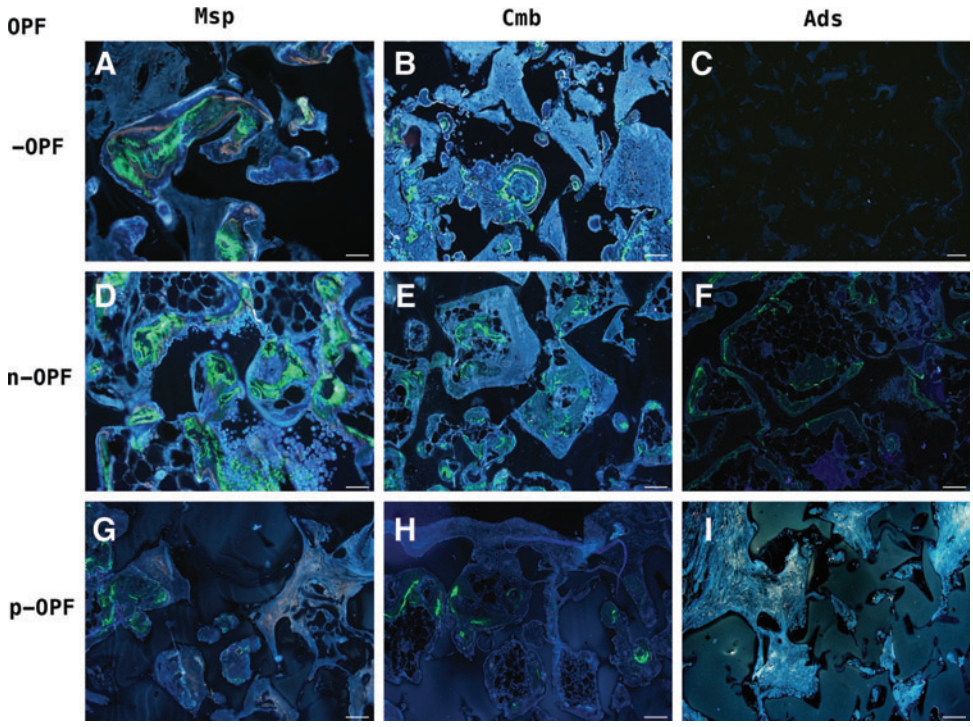

FIG. 8. Fluorescence imaging of histological samples of BMP-2 containing OPF composites. Fluorescence markers calcein *green* (*green*) and tetracycline (*orange*) showed aspects of woven **(D, E, G, and H)** and lamellar **(A, B, and F)** bone disposition starting at various locations both early (3 weeks, calcein) and late (6 weeks, tetracycline) in the pores of -OPF-Msp, -OPF-Cmb, all n-OPF, p-OPF-Msp, and p-OPF-Cmb hydrogels **(A, B, and D–H)**. No fluorescence markers were observed in -OPF-Ads and p-OPF-Ads (**C, I**). Scale bars represent 100 μm **(B, C, and E–I)** and 50 μm **(A, D)**. Msp, 100% BMP-2 loaded in PLGA microspheres; Cmb, 50% BMP-2 loaded in PLGA microspheres, 50% BMP-2 adsorbed on the hydrogel; Ads, 100% BMP-2 loaded on the hydrogel; -OPF, unmodified OPF; n-OPF, negatively charged OPF; p-OPF, positively charged OPF. Color images are available online.

relationship between BMP-2 release and bone formation in biomaterials with similar chemistry and structure.[4,56] Previous studies of our group showed the profound effect of BMP-2 release profiles on *in vivo* bone formation.[30,57] Whereas the amount subcutaneous bone formation was correlated with BMP-2 burst release in phosphate-modified OPF hydrogels, no difference was observed between BMP-2 burst release and sustained release in an orthotopic defect site. Although the effect of release on bone formation may differ between different biomaterials and application sites, the results of this study clearly show that tailoring release within the biomaterial is important to optimize bone formation.

Charge influenced BMP-2 release and hence may have affected bone formation

For microsphere-encapsulated BMP-2, positive charge decreased BMP-2 burst release and released the BMP-2 in a more sustained manner compared with neutral and negative charge in OPF composites. As shown by the effect of different BMP-2 loading methods, a more sustained release can also enhance bone formation in these composites. However, n-OPF generated more bone formation compared with neutral and positively charged OPF-MAE within all BMP-2 loading methods. Altogether, these findings indicate that negative charge was the major determinant in BMP-2-induced bone formation. Apart from influencing bone formation *in vivo*, differentially charged biomaterial surfaces affect BMP-2 release kinetics *in vitro* and *in vivo*.

Charge modifications affected the in vitro *and* in vivo *BMP-2 release differently*

Whereas n-OPF resulted in a significantly lower burst release and higher subsequent sustained release compared with the other charge modifications *in vitro*, p-OPF resulted in a significantly lower burst release and higher subsequent sustained release compared with other charge modifications *in vivo*. These differences highlight that *in vitro* conditions do not mimic the complexity of the chemical, mechanical, electrical, and biological *in vivo* environment. Specific proteins and cells could have influenced the scaffold BMP-2 binding in the *in vivo* environment.[58,59] So far, studies investigating *in vivo* BMP-2 release kinetics are sparse and protein release from biomaterials is usually studied in an *in vitro* environment. Although *in vitro* studies provide useful information on scaffold/protein interactions, these results and previous studies[3,32,51,56,60–64] highlight that the need for careful data interpretation is warranted.

Compared with the BMP-2 loading method, biomaterial surface charge had limited effect on in vivo *BMP-2 release kinetics*

Fully adsorbing BMP-2 on the hydrogel surface resulted in large burst release (>78%) after 3 days without relevant

differences between the differently charged surfaces. Since the BMP-2 is adsorbed on the hydrogel, protein binding is dependent on physiochemical interactions and ionic complexation, hence highly sensitive to environmental conditions.[65] No relevant differences in this study between the charged surfaces indicate that rapid desorption and ion exchange in the *in vivo* environment override the effect of differential protein ionic complexation. Previous studies show that adsorption on phosphorylated OPF, poly(propylene fumarate), and collagen generated similar large burst releases (>70%) after 3 days.[30,55,66] Furthermore, when BMP-2 was adsorbed on acidic and basic gelatin, large burst releases (>90%) after 3 days were observed without relevant differences between the charged biomaterials.[63] On the contrary, studies on several ceramics showed that protein adsorption could also generate a more sustained *in vivo* release due to physiochemical interactions between BMP-2 and biomaterials.[39,67]

Microsphere encapsulation and subsequent embedding in the hydrogel matrix resulted in significant reduction of the burst release (<66%) and subsequent sustained release for all charge modifications. This is in line with previous studies investigating *in vivo* BMP-2 release from PLGA microspheres.[30,32,56] While neutral and negatively charged hydrogels generated similar BMP-2 release kinetics, positively charged hydrogels showed significantly lower burst releases (<43%) for microsphere-encapsulated BMP-2. By embedding the PLGA microspheres in different hydrogels, the BMP-2 was physically entrapped, creating an extra diffusion barrier.

Since BMP-2 adsorption on the differentially charged OPF showed no relevant differences in BMP-2 release kinetics, degradation of the additional diffusion barrier may cause this difference. This was also seen in previous research, where BMP-2 encapsulated in PLGA microspheres with similar characteristics embedded in different biomaterials resulted in various BMP-2 release profiles.[32,51,54,62,68,69] The difference in degradation rate between the differentially charged OPF remains to be investigated.

Conclusion

In conclusion, negative charge enhanced bone formation compared with neutral and positive charge in OPF composites. The enhanced bone formation was seen for all three loading methods and subsequent BMP-2 release profiles. Although biomaterial surface charge had limited effect on BMP-2 release, bone formation was also improved by sustained release of BMP-2 from PLGA microspheres within the OPF hydrogel.

Acknowledgments

The authors thank Dr. Nynke Ankringa, ECVP board eligible veterinary pathologist of the Faculty of Veterinary Medicine at the University of Utrecht, for her assistance during the histological analysis. They also thank James L. Herrick and Carl T. Gustafson of Mayo Clinic for technical support. The authors also acknowledge the National Institutes of Health (R01 AR45871 and R01 EB03060), the AO Foundation (AO startup grant S-15-46K), the Dutch Arthritis Foundation (LLP22), and the Anna-NOREF foundation for their financial support.

Disclosure Statement

No competing financial interests exist.

Supplementary Material

Supplementary Figure S1

References

1. Seeherman, H., Li, R., and Wozney, J. A review of preclinical program development for evaluating injectable carriers for osteogenic factors. J Bone Joint Surg Am **85(Suppl. 3)**, 96, 2003.
2. Putney, S.D., and Burke, P.A. Improving protein therapeutics with sustained-release formulations. Nat Biotechnol **16**, 153, 1998.
3. Rodríguez-Évora, M., Delgado, A., Reyes, R., *et al.* Osteogenic effect of local, long versus short term BMP-2 delivery from a novel SPU-PLGA-betaTCP concentric system in a critical size defect in rats. Eur J Pharm Sci **49**, 873, 2013.
4. Yamamoto, M., Takahashi, Y., and Tabata, Y. Controlled release by biodegradable hydrogels enhances the ectopic bone formation of bone morphogenetic protein. Biomaterials **24**, 4375, 2003.
5. Yamamoto, M., Tabata, Y., and Ikada, Y. Ectopic bone formation induced by biodegradable hydrogels incorporating bone morphogenetic protein. J Biomater Sci Polym Ed **9**, 439, 1998.
6. Furth, M.E., Atala, A., and Van Dyke, M.E. Smart biomaterials design for tissue engineering and regenerative medicine. Biomaterials **28**, 5068, 2007.
7. Langer, R., Cima, L.G., Tamada, J.A., and Wintermantel, E. Future directions in biomaterials. Biomaterials **11**, 738, 1990.
8. Choudhary, S., Haberstroh, K.M., and Webster, T.J. Enhanced functions of vascular cells on nanostructured Ti for improved stent applications. Tissue Eng **13**, 1421, 2007.
9. Lu, J., Rao, M.P., MacDonald, N.C., Khang, D., and Webster, T.J. Improved endothelial cell adhesion and proliferation on patterned titanium surfaces with rationally designed, micrometer to nanometer features. Acta Biomater **4**, 192, 2008.
10. Zhang, Y.M., Bataillon-Linez, P., Huang, P., *et al.* Surface analyses of micro-arc oxidized and hydrothermally treated titanium and effect on osteoblast behavior. J Biomed Mater Res A **68**, 383, 2004.
11. Fukada, E., and Yasuda, I. On the piezoelectric effect of bone. J Phys Soc Jpn **12**, 1158, 1957.
12. Yasuda, I. Electrical callus and callus formation by electret. Clin Orthop Relat Res **124**, 53, 1977.
13. Horii, A., Wang, X., Gelain, F., and Zhang, S. Biological designer self-assembling peptide nanofiber scaffolds significantly enhance osteoblast proliferation, differentiation and 3-D migration. PLoS One **2**, e190, 2007.
14. Saito, A., Suzuki, Y., Ogata, S.I., Ohtsuki, C., and Tanihara, M. Accelerated bone repair with the use of a synthetic BMP-2-derived peptide and bone-marrow stromal cells. J Biomed Mater Res A **72a**, 77, 2005.
15. Salinas, C.N., and Anseth, K.S. The enhancement of chondrogenic differentiation of human mesenchymal stem

cells by enzymatically regulated RGD functionalities. Biomaterials **29**, 2370, 2008.
16. King, T.G., Preston, M.E., Murphy, B.J.M., and Cannell, D.S. Piezoelectric ceramic actuators: a review of machinery applications. Precis Eng **12**, 131, 1990.
17. Yasuda, I. Piezoelectricity of living bone. J Kyoto Pref Univ Med **53**, 325, 1953.
18. Yasuda, I. The classic fundamental aspects of fracture treatment. Clin Orthop Relat Res **124**, 5, 1977.
19. Fukada, E. Piezoelectric properties of organic polymers. Ann N Y Acad Sci **238**, 7, 1974.
20. Bassett, C.A.L., Pawluk, R.J., and Becker, R.O. Effects of electric currents on bone in vivo. Nature **204**, 652, 1964.
21. Park, J.B., von Recum, A.F., Kenner, G.H., Kelly, B.J., Coffeen, W.W., and Grether, M.F. Piezoelectric ceramic implants: a feasibility study. J Biomed Mater Res **14**, 269, 1980.
22. Feng, J., Yuan, H., and Zhang, X. Promotion of osteogenesis by a piezoelectric biological ceramic. Biomaterials **18**, 1531, 1997.
23. Ikada, Y., Shikinami, Y., Hara, Y., Tagawa, M., and Fukada, E. Enhancement of bone formation by drawn poly(L-lactide). J Biomed Mater Res **30**, 553, 1996.
24. Inoue, S., Ohashi, T., Yasuda, I., and Fukada, E. Electret induced callus formation in the rat. Clin Orthop Relat Res **124**, 57, 1977.
25. Yamashita, K., Oikawa, N., and Umegaki, T. Acceleration and deceleration of bone-like crystal growth on ceramic hydroxyapatite by electric poling. Chem Mater **8**, 2697, 1996.
26. Ohgaki, M., Kizuki, T., Katsura, M., and Yamashita, K. Manipulation of selective cell adhesion and growth by surface charges of electrically polarized hydroxyapatite. J Biomed Mater Res **57**, 366, 2001.
27. Nakamura, S., Kobayashi, T., and Yamashita, K. Numerical osteobonding evaluation of electrically polarized hydroxyapatite ceramics. J Biomed Mater Res A **68**, 90, 2004.
28. Dadsetan, M., Pumberger, M., Casper, M.E., *et al.* The effects of fixed electrical charge on chondrocyte behavior. Acta Biomater **7**, 2080, 2011.
29. Dadsetan, M., Knight, A.M., Lu, L., Windebank, A.J., and Yaszemski, M.J. Stimulation of neurite outgrowth using positively charged hydrogels. Biomaterials **30**, 3874, 2009.
30. Olthof, M.G.L., Kempen, D.H.R., Liu, X., *et al.* Bone morphogenetic protein-2 release profile modulates bone formation in phosphorylated hydrogel. J Tissue Eng Regen Med **12**, 1339, 2018.
31. Poduslo, J.F., Curran, G.L., and Berg, C.T. Macromolecular permeability across the blood-nerve and blood–brain barriers. Proc Natl Acad Sci U S A **91**, 5705, 1994.
32. Kempen, D.H., Lu, L., Hefferan, T.E., *et al.* Retention of in vitro and in vivo BMP-2 bioactivities in sustained delivery vehicles for bone tissue engineering. Biomaterials **29**, 3245, 2008.
33. Kempen, D.H., Lu, L., Classic, K.L., *et al.* Non-invasive screening method for simultaneous evaluation of in vivo growth factor release profiles from multiple ectopic bone tissue engineering implants. J Control Release **130**, 15, 2008.
34. Shive, M.S., and Anderson, J.M. Biodegradation and biocompatibility of PLA and PLGA microspheres. Adv Drug Deliv Rev **28**, 5, 1997.
35. Dadsetan, M., Szatkowski, J.P., Yaszemski, M.J., and Lu, L. Characterization of photo-cross-linked oligo[poly(ethylene glycol) fumarate] hydrogels for cartilage tissue engineering. Biomacromolecules **8**, 1702, 2007.
36. Thies, R.S., Bauduy, M., Ashton, B.A., Kurtzberg, L., Wozney, J.M., and Rosen, V. Recombinant human bone morphogenetic protein-2 induces osteoblastic differentiation in W-20-17 stromal cells. Endocrinology **130**, 1318, 1992.
37. Villanueva, A.R., and Mehr, L.A. Modifications of the Goldner and Gomori one-step trichrome stains for plastic-embedded thin sections of bone. Am J Med Technol **43**, 536, 1977.
38. Gruber, R., Weich, H.A., Dullin, C., and Schliephake, H. Ectopic bone formation after implantation of a slow release system of polylactic acid and rhBMP-2. Clin Oral Implants Res **20**, 24, 2009.
39. Tazaki, J., Murata, M., Akazawa, T., *et al.* BMP-2 release and dose–response studies in hydroxyapatite and beta-tricalcium phosphate. Biomed Mater Eng **19**, 141, 2009.
40. Bodhak, S., Bose, S., and Bandyopadhyay, A. Role of surface charge and wettability on early stage mineralization and bone cell-materials interactions of polarized hydroxyapatite. Acta Biomater **5**, 2178, 2009.
41. Bodhak, S., Bose, S., and Bandyopadhyay, A. Electrically polarized HAp-coated Ti: in vitro bone cell-material interactions. Acta Biomater **6**, 641, 2010.
42. Tarafder, S., Bodhak, S., Bandyopadhyay, A., and Bose, S. Effect of electrical polarization and composition of biphasic calcium phosphates on early stage osteoblast interactions. J Biomed Mater Res B Appl Biomater **97**, 306, 2011.
43. Kizuki, T., Ohgaki, M., Katsura, M., *et al.* Effect of bone-like layer growth from culture medium on adherence of osteoblast-like cells. Biomaterials **24**, 941, 2003.
44. Nakamura, S., Kobayashi, T., and Yamashita, K. Extended bioactivity in the proximity of hydroxyapatite ceramic surfaces induced by polarization charges. J Biomed Mater Res **61**, 593, 2002.
45. Nakamura, M., Sekijima, Y., Nakamura, S., Kobayashi, T., Niwa, K., and Yamashita, K. Role of blood coagulation components as intermediators of high osteoconductivity of electrically polarized hydroxyapatite. J Biomed Mater Res A **79**, 627, 2006.
46. Davies, J.E., Causton, B., Bovell, Y., Davy, K., and Sturt, C.S. The migration of osteoblasts over substrata of discrete surface charge. Biomaterials **7**, 231, 1986.
47. Farbod, K., Nejadnik, M.R., Jansen, J.A., and Leeuwenburgh, S.C. Interactions between inorganic and organic phases in bone tissue as a source of inspiration for design of novel nanocomposites. Tissue Eng Part B Rev **20**, 173, 2014.
48. Toworfe, G.K., Composto, R.J., Shapiro, I.M., and Ducheyne, P. Nucleation and growth of calcium phosphate on amine-, carboxyl- and hydroxyl-silane self-assembled monolayers. Biomaterials **27**, 631, 2006.
49. Itoh, S., Nakamura, S., Nakamura, M., Shinomiya, K., and Yamashita, K. Enhanced bone ingrowth into hydroxyapatite with interconnected pores by electrical polarization. Biomaterials **27**, 5572, 2006.
50. Hosseinkhani, H., Hosseinkhani, M., Khademhosseini, A., and Kobayashi, H. Bone regeneration through controlled release of bone morphogenetic protein-2 from 3-D tissue engineered nano-scaffold. J Control Release **117**, 380, 2007.
51. Hernández, A., Sánchez, E., Soriano, I., Reyes, R., Delgado, A., and Évora, C. Material-related effects of BMP-2

delivery systems on bone regeneration. Acta Biomater **8**, 781, 2012.
52. Takahashi, Y., Yamamoto, M., and Tabata, Y. Enhanced osteoinduction by controlled release of bone morphogenetic protein-2 from biodegradable sponge composed of gelatin and beta-tricalcium phosphate. Biomaterials **26**, 4856, 2005.
53. Takita, H., Vehof, J.W., Jansen, J.A., *et al.* Carrier dependent cell differentiation of bone morphogenetic protein-2 induced osteogenesis and chondrogenesis during the early implantation stage in rats. J Biomed Mater Res A **71**, 181, 2004.
54. Bodde, E.W., Boerman, O.C., Russel, F.G., Mikos, A.G., Spauwen, P.H., and Jansen, J.A. The kinetic and biological activity of different loaded rhBMP-2 calcium phosphate cement implants in rats. J Biomed Mater Res A **87**, 780, 2008.
55. Uludag, H., D'Augusta, D., Golden, J., *et al.* Implantation of recombinant human bone morphogenetic proteins with biomaterial carriers: a correlation between protein pharmacokinetics and osteoinduction in the rat ectopic model. J Biomed Mater Res **50**, 227, 2000.
56. van de Watering, F.C., Molkenboer-Kuenen, J.D., Boerman, O.C., van den Beucken, J.J., and Jansen, J.A. Differential loading methods for BMP-2 within injectable calcium phosphate cement. J Control Release **164**, 283, 2012.
57. Olthof, M.G.L., Lu, L., Tryfonidou, M.A., *et al.* The osteoinductive effect of controlled BMP-2 release is location-dependent. Tissue Eng Part A **25**, 193, 2019.
58. Xia, Z., and Triffitt, J.T. A review on macrophage responses to biomaterials. Biomed Mater **1**, R1, 2006.
59. Baxter, F.R., Bowen, C.R., Turner, I.G., and Dent, A.C. Electrically active bioceramics: a review of interfacial responses. Ann Biomed Eng **38**, 2079, 2010.
60. Piskounova, S., Gedda, L., Hulsart-Billström, G., Hilborn, J., and Bowden, T. Characterization of recombinant human bone morphogenetic protein-2 delivery from injectable hyaluronan-based hydrogels by means of 125I-radiolabelling. J Tissue Eng Regen Med **8**, 821, 2014.
61. Ruhé, P.Q., Boerman, O.C., Russel, F.G., Mikos, A.G., Spauwen, P.H., and Jansen, J.A. In vivo release of rhBMP-2 loaded porous calcium phosphate cement pretreated with albumin. J Mater Sci Mater Med **17**, 919, 2006.
62. Woo, B.H., Fink, B.F., Page, R., *et al.* Enhancement of bone growth by sustained delivery of recombinant human bone morphogenetic protein-2 in a polymeric matrix. Pharm Res **18**, 1747, 2001.
63. Yamamoto, M., Ikada, Y., and Tabata, Y. Controlled release of growth factors based on biodegradation of gelatin hydrogel. J Biomater Sci Polym Ed **12**, 77, 2001.
64. Olthof, M.G.L., Tryfonidou, M.A., Dadsetan, M., *et al.* In vitro and in vivo correlation of bone morphogenetic protein-2 release profiles from complex delivery vehicles. Tissue Eng Part C Methods **24**, 379, 2018.
65. Luginbuehl, V., Meinel, L., Merkle, H.P., and Gander, B. Localized delivery of growth factors for bone repair. Eur J Pharm Biopharm **58**, 197, 2004.
66. Patel, Z.S., Yamamoto, M., Ueda, H., Tabata, Y., and Mikos, A.G. Biodegradable gelatin microparticles as delivery systems for the controlled release of bone morphogenetic protein-2. Acta Biomater **4**, 1126, 2008.
67. Louis-Ugbo, J., Kim, H.S., Boden, S.D., *et al.* Retention of 125I-labeled recombinant human bone morphogenetic protein-2 by biphasic calcium phosphate or a composite sponge in a rabbit posterolateral spine arthrodesis model. J Orthop Res **20**, 1050, 2002.
68. Reyes, R., Delgado, A., Sánchez, E., Fernández, A., Hernández, A., and Evora, C. Repair of an osteochondral defect by sustained delivery of BMP-2 or TGFbeta1 from a bilayered alginate-PLGA scaffold. J Tissue Eng Regen med **8**, 521, 2014.
69. Reyes, R., Delgado, A., Solis, R., *et al.* Cartilage repair by local delivery of transforming growth factor-beta1 or bone morphogenetic protein-2 from a novel, segmented polyurethane/polylactic-co-glycolic bilayered scaffold. J Biomed Mater Res A **102**, 1110, 2014.

Address correspondence to:
Lichun Lu, PhD
Department of Physiology and Biomedical Engineering
Mayo Clinic College of Medicine
200 First Street SW, MS 3-69
Rochester, MN 55905

E-mail: lu.lichun@mayo.edu

Received: May 27, 2018
Accepted: November 6, 2018
Online Publication Date: June 14, 2019